Iterative positioning of microphone arrays for acoustic imaging

Laurent Gilquin, Pierre Lecomte, Jérôme Antoni, Thibaut Le Magueresse, Clément Marteau

Iterative positioning of microphone arrays for acoustic imaging

Laurent Gilquin[a], Pierre Lecomte[a], Jérôme Antoni[a], Thibaut le Magueresse[b], Clément Marteau[c]

[a] *Univ Lyon, INSA-Lyon, Laboratoire Vibrations Acoustique, F-69621 Villeurbanne, France*
[b] *MicrodB, 28 Chemin du Petit Bois, Ecully, France*
[c] *Univ Lyon, Université Claude Bernard Lyon 1, CNRS UMR 5208, Institut Camille Jordan, F-69622 Villeurbanne, France*

Abstract

For the characterization of acoustic sources, a common approach is to retro-propagate the sound pressure measured with a microphone array, which is often performed through the resolution of an inverse problem. The ill-posed nature of this problem, as well as the limited number of measurements, are known to reduce the quality of the source reconstruction. A practical solution to these limitations is to increase the number of measurements with new array placements. However, finding the best array positions is not a straightforward process. The present paper tackles this issue by introducing a sequential approach that select at each iteration the optimal array placement. The proposed approach builds on two features rooted in a Bayesian framework: an inverse method called "Bayesian focusing" and a Bayesian search criterion based on the Kullback-Leibler divergence. Simulations results for the characterization of a directive source are used to illustrate the performance of the proposed approach. It is shown that for a fixed number of iterations, the proposed approach performs better than ones where the successive placements are randomly selected around the source, or others where the placements follow a deterministic spherical grid pattern.

1. Introduction

One of the objects of acoustic imaging is to characterize an unknown source field through the retro-propagation of acoustic pressures measured with an array of microphones. This is often performed through solving an inverse problem, with the aim of identifying either the source location, its

strength or both. However, it is well-known that the quality of the reconstructed source field is impaired by several factors, among which the ill-posed nature of the inverse problem and the limited number of available microphones. This limits the amount of information that can be recovered by measurements, which can be critical in industrial settings where the sharpness of the mesh modeling the surface of interest is high, the radiation angle covered by the array is small and the number of microphones it contains is restricted by a budget.

To increase the amount of information required for reaching an accurate acoustic imaging, a practical solution is to use either multiple microphone arrays or a single one to sequentially acquire new set of measurements. In the latter case, the array is moved at each iteration and additional fixed reference microphones are used to synchronize the measurements. Such an approach allows restoring the well-posedness of the inverse problem, if the microphone array placements are suitable. In practice, the array positions are usually chosen based on engineering expertise which may not be optimal. The aim of the present work is to find the best (in a sens to be defined) placements of the array such that the resulting measurements will be the most informative about the source target.

Previous work addressing this issue have already been carried out in several papers. In structural dynamics for instance, information theoretic approaches have been applied to find an optimal selection of sensors placement in a structure of interest. The approaches stand out from one each other according to the optimal criterion used to select the best placements. Notable ones are: norms of the Fisher information matrix [1] - [2], expected Bayesian loss function [3], information entropy index [4] - [5] . The issue at hand has also been tackled in other acoustic fields: modal identification [6] and design of spherical microphone arrays [7] - [8].

The present paper introduces an automatic and efficient approach to sequentially select optimal positions of microphone arrays. The proposed approach is rooted in a Bayesian framework and builds on two features: an inverse method called "Bayesian focusing"[9] to update the source model (that is to estimate the source field based on new measurements), and an information theory criterion based on the Kullback-Leibler divergence [10] to find the next optimal position. The search criterion in question is one of many introduced in Bayesian Experimental Design (BED) [11]. Several applications of BED have been conducted outside of acoustics, notably in chemical kinetics [12], in pharmacokinetic [13] or in visual perception [14]. Hence, the approach introduced in the present paper can be viewed as an application of BED (more specifically sequential BED) in acoustics, which

up to our knowledge has not yet been proposed. It should also reveal itself particularly useful for industrial applications as it offers a trade-off between the cost of an experiment and the information gained from additional microphone arrays about the source target, that is to make cost-effective decisions regarding optimal experimentation.

The outline of this paper is the following. The two features of the proposed sequential approach are introduced in Section 2. Section 3 provides an in-depth presentation of the sequential approach together the proposed algorithm. Section 4 illustrates the proposed approach with a real scope numerical application.

2. Backgrounds

Throughout this paper, a vector is denoted by a lower case bold letter (*e.g.* $\mathbf{v}$) and a matrix is denoted by a capital bold letter (*e.g.* $\mathbf{M}$).

2.1. Bayesian focusing

Bayesian focusing is one of the numerous imaging method that can be used to solve the problem of reconstructing an acoustic source. In the frequency domain (dependence on frequency f is omitted for notational simplicity), this problem can be formulated as a linear relationship linking the set of measurements $\widetilde{\boldsymbol{p}}$ captured by a microphone array to the source field $\boldsymbol{q}$ to be reconstructed. The microphones positions are denoted by $\boldsymbol{r}_i$, $i = 1, \ldots, M$ and the surface Γ on which the source field is to be reconstructed is discretized into a set of points $\boldsymbol{r}$. Then, the linear relationship is completely determined by:

$$\widetilde{p}(\boldsymbol{r}_i) = \sum_{\boldsymbol{r}\in\Gamma} G(\boldsymbol{r}_i|\boldsymbol{r}) q(\boldsymbol{r}) + n_i \ , \qquad i = 1, \ldots, M \ , \tag{1}$$

where $G(\boldsymbol{r}_i|\boldsymbol{r})$ denotes the Green function between the surface Γ, at point $\boldsymbol{r}$, and the microphone position $\boldsymbol{r}_i$, and $\boldsymbol{n} = (n_1, \ldots, n_M)$ is the vector of measurement noises. Equation (1) can be rewritten in matrix form to consider all measurements at once:

$$\widetilde{\boldsymbol{p}} = \boldsymbol{G}\boldsymbol{q} + \boldsymbol{n} \ . \tag{2}$$

The challenge at hand is to recover the source field $\boldsymbol{q}$ from (2). This task corresponds to an inverse problem, since one needs to provide an inversion of the operator $\boldsymbol{G}$. Such a problem is typically ill-posed as existence, uniqueness and stability of the solution are not guaranteed.

Bayesian focusing is an inverse method that has proved to be efficient on a wide range of applications. It belongs to the class of "matrix inversion" methods and is noteworthy for bringing an unifying framework, rooted in a Bayesian formalism, for acoustics inverse methods. The main results of Bayesian focusing [9] are outlined below.

Equation (2) is handled by viewing $\boldsymbol{q}$ and $\widetilde{\boldsymbol{p}}$ as vectors of complex random variables and assigning to them probability density functions (PDF). To this end, $\boldsymbol{p}$ is substituted for $\widetilde{\boldsymbol{p}}$ to differentiate between the random variables and their realizations. Additionally, the notation [.] is introduced to denote the PDF of a random variable. The PDFs of interest are: the likelihood $[\boldsymbol{p}|\boldsymbol{q}]$ expressing the probability distribution of the measurements given $\boldsymbol{q}$, and the prior $[\boldsymbol{q}]$ that summarizes any available information about the source field. The solution of the inverse problem is characterized by the posterior probability distribution $[\boldsymbol{q}|\boldsymbol{p}]$. It is expressed by Bayes rule:

$$[\boldsymbol{q}|\boldsymbol{p}] = \frac{[\boldsymbol{p}|\boldsymbol{q}]\,[\boldsymbol{q}]}{[\boldsymbol{p}]} \ , \tag{3}$$

where $[\boldsymbol{p}]$ is the evidence. The likelihood and the prior probability distributions are selected as in [9]. First, the noise $\boldsymbol{n}$ is assumed to follow a circularly-symmetric[1] complex normal distribution [15]:

$$[\boldsymbol{n}] = \mathcal{CN}(\boldsymbol{0}, \beta^2 I_{\boldsymbol{n}}) \ , \tag{4}$$

where β^2 characterizes the unknown expected noise energy, $I_{\boldsymbol{n}}$ is the identity matrix and the symbol $\mathcal{CN}$ stands for complex normal (in the frequency domain, all quantities are assumed complex-valued). As a result, the likelihood follows a circular complex normal distribution:

$$[\boldsymbol{p}|\boldsymbol{q}] = \mathcal{CN}(\boldsymbol{G}\boldsymbol{q}, \beta^2 I_{\boldsymbol{n}}) \ . \tag{5}$$

The prior is also assumed to follow a circularly-symmetric complex normal distribution:

$$[\boldsymbol{q}] = \mathcal{CN}(\boldsymbol{0}, \alpha^2 I_{\boldsymbol{q}}) \ , \tag{6}$$

where α^2 characterizes the unknown source energy. As a consequence of these assumptions, the evidence can be explicitly calculated. It follows a circularly-symmetric complex normal distribution as well:

$$[\boldsymbol{p}] = \mathcal{CN}(\boldsymbol{0}, \alpha^2 \boldsymbol{G}\boldsymbol{G}^{\mathsf{H}} + \beta^2 I_{\boldsymbol{n}}) \ , \tag{7}$$

[1] circular(-ly): the real and imaginary parts are independent real normal random variables with the same variance, symmetric: zero mean.

where the superscript $^{\mathsf{H}}$ stands for the conjugate transpose operator. Finally, the posterior is derived from Eqs. (3)-(7) and reads:

$$[\boldsymbol{q}|\boldsymbol{p}] = \mathcal{CN}(\mu_{\boldsymbol{q}}, \Sigma_{\boldsymbol{q}}) \ ,$$

with:

$$\mu_{\boldsymbol{q}} = \alpha^2 \boldsymbol{G}^{\mathsf{H}} (\boldsymbol{G}\boldsymbol{G}^{\mathsf{H}} + \eta^2 I_{\boldsymbol{n}})^{-1} \boldsymbol{p} \ , \qquad \Sigma_{\boldsymbol{q}} = (\alpha^{-2} I_{\boldsymbol{q}} + \beta^{-2} \boldsymbol{G}^{\mathsf{H}} \boldsymbol{G})^{-1} \ . \tag{8}$$

$\mu_{\boldsymbol{q}}$ is called the maximum a posteriori (MAP) estimator which fits the measurements $\boldsymbol{p}$ with the highest probability. The MAP identifies as the solution of a generalized Thikonov regularization [16] where $\eta^2 = \beta^2/\alpha^2$ plays the role of the regularization parameter. Note that since α^2 and β^2 are unknown variables, the parameter η^2 has to be calibrated. An estimation procedure of η^2, rooted in the posterior distribution, is introduced in [17].

2.2. Bayesian experimental design

This section reviews the probability framework called Bayesian experimental design and from which the search criterion of the proposed sequential approach is derived. As BED is also based on Bayesian inference, the notations $\boldsymbol{p}$ and $\boldsymbol{q}$ introduced in Section 2.1 are kept.

From here on, the position and orientation of the microphone array are modeled by a vector $\boldsymbol{d}$ expressed in the main coordinate system $(O, \boldsymbol{x}, \boldsymbol{y}, \boldsymbol{z})$ shown in Fig. 1. This vector contains the coordinates and orientation angles of the microphone array, that are modeled by n_d real random variables.

For a given experiment performed at conditions $\boldsymbol{d}$, one obtains a vector of measurements $\widetilde{\boldsymbol{p}}$, that is a set of realizations of $\boldsymbol{p}$. Then, Bayes rule is used to inform about the state of the source field $\boldsymbol{q}$:

$$[\boldsymbol{q}|\boldsymbol{p}, \boldsymbol{d}] = \frac{[\boldsymbol{p}|\boldsymbol{q}, \boldsymbol{d}]\,[\boldsymbol{q}|\boldsymbol{d}]}{[\boldsymbol{p}|\boldsymbol{d}]} \ . \tag{9}$$

In the context studied here, it is assumed that prior knowledge about the source field $\boldsymbol{q}$ are independent of the experimental conditions $\boldsymbol{d}$. This leads to the simplification $[\boldsymbol{q}|\boldsymbol{d}] = [\boldsymbol{q}]$. In the following, Θ will denote the support of the prior distribution $[\boldsymbol{q}]$ and $\mathcal{P}$ the support of the evidence $[\boldsymbol{p}|\boldsymbol{d}]$.

2.2.1. Expected utility

The aim of BED is to maximize the information brought by a set of measurements about the state of the model $\boldsymbol{q}$. In the present context, this can be rephrased as finding an optimal position of the microphone array at

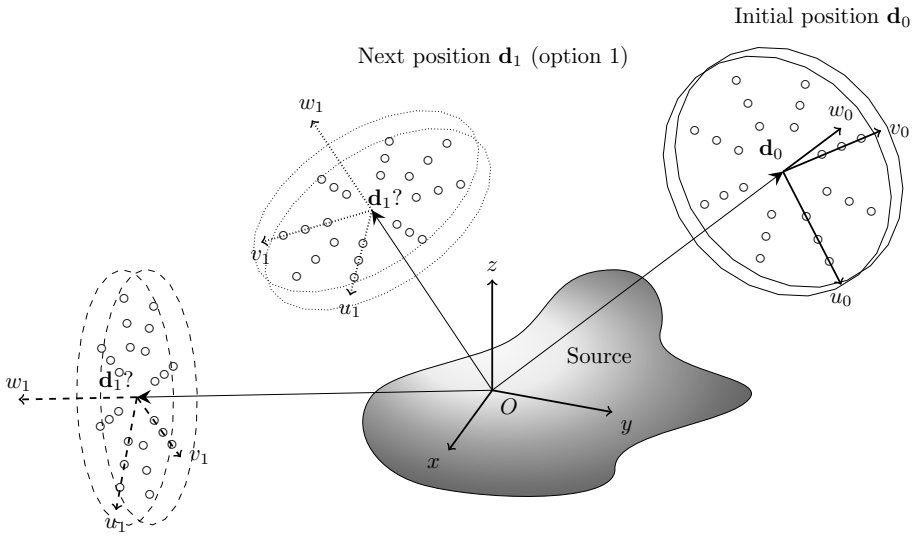

Figure 1: Schematic of the proposed sequential method: the microphone array is placed at an initial position $\boldsymbol{d}_0$ (solid line setup on top right). Among several options for the next position $\boldsymbol{d}_1$ (dotted and dashed setups on left side), the algorithm selects the one that brings the most information for the Bayesian focusing.

which measurements will be performed to further improve the reconstruction of the source field.

Following the decision theory introduced by Lindley [18], the choice of the optimal position, hereafter noted by $\boldsymbol{d}^\star$, is defined as the one maximizing a quantity called "expected utility",

$$\boldsymbol{d}^\star = \underset{\boldsymbol{d} \,\in\, \mathbb{R}^{n_d}}{\operatorname{argmax}} \; \mathbb{E}_{\boldsymbol{p}|\boldsymbol{d}} \left[u(\boldsymbol{d}, \boldsymbol{p}, \boldsymbol{q}) \right] = \underset{\boldsymbol{d} \,\in\, \mathbb{R}^{n_d}}{\operatorname{argmax}} \; \mathrm{U}(\boldsymbol{d}) \;, \tag{10}$$

$$\mathrm{U}(\boldsymbol{d}) = \int_{\mathcal{P}} \int_{\Theta} u(\boldsymbol{d}, \boldsymbol{p}, \boldsymbol{q}) \, [\boldsymbol{p}, \boldsymbol{q}|\boldsymbol{d}] \, d\boldsymbol{q} d\boldsymbol{p} \;, \tag{11}$$

where $\mathrm{U}(\boldsymbol{d})$ is the expected utility associated to a utility function $u(\boldsymbol{d}, \boldsymbol{p}, \boldsymbol{q})$. The choice of the utility function should reflect the objective sought by the experimenter as it will be used to gauge the usefulness of obtaining a new outcome $\boldsymbol{p}$, at conditions $\boldsymbol{d}$, given a model state $\boldsymbol{q}$. Since $\boldsymbol{p}$ and $\boldsymbol{q}$ are unknown before the experiment is carried out, the expectation of u is taken over both spaces $\mathcal{P}$ and Θ.

2.2.2. Kullback-Leibler divergence

As suggested in [19], a classical choice for the utility function is the Kullback-Leibler (KL) divergence of the prior from the posterior distribution:

$$u(\boldsymbol{d}, \boldsymbol{p}, \boldsymbol{q}) = D_{\mathrm{KL}}([\boldsymbol{q}|\boldsymbol{p}, \boldsymbol{d}] \parallel [\boldsymbol{q}]) = \int_{\Theta} [\boldsymbol{q}|\boldsymbol{p}, \boldsymbol{d}] \ln \left(\frac{[\boldsymbol{q}|\boldsymbol{p}, \boldsymbol{d}]}{[\boldsymbol{q}]} \right) d\boldsymbol{q} \ . \tag{12}$$

The KL divergence is non-symmetric, non-negative and measures the difference in information between two distributions.

Investigating the KL divergence between posterior and prior PDFs will indicate whether acquiring new measurements at the position $\boldsymbol{d}$ is meaningful or not. If the KL divergence is close to zero, then the posterior and prior are nearly identical, that is the position $\boldsymbol{d}$ will not bring useful measurements. On the other hand, if the KL divergence is large, then the position $\boldsymbol{d}$ is relevant for the reconstruction of the source field.

Equation (12) shows that the KL divergence is not a function of $\boldsymbol{q}$, which leads to the simplification $u(\boldsymbol{d}, \boldsymbol{p}, \boldsymbol{q}) = u(\boldsymbol{d}, \boldsymbol{p})$. Then, inserting Eq. (12) into (11) yields:

$$\mathrm{U}(\boldsymbol{d}) = \int_{\mathcal{P}} u(\boldsymbol{d}, \boldsymbol{p}) \, [\boldsymbol{p}|\boldsymbol{d}] \, d\boldsymbol{p} = \mathbb{E}_{\boldsymbol{p}|\boldsymbol{d}} \left[D_{\mathrm{KL}}([\boldsymbol{q}|\boldsymbol{p}, \boldsymbol{d}] \parallel [\boldsymbol{q}]) \right] \ . \tag{13}$$

Equation (13) holds the following interpretation: a large value of the expected value $\mathrm{U}(\boldsymbol{d})$ implies that, on the average, the measurements $\boldsymbol{p}$ obtained at the position $\boldsymbol{d}$ are more likely to be informative about the source field $\boldsymbol{q}$. Hence, the optimal position $\boldsymbol{d}^\star$ is the one that will maximize the information gain on average:

$$\boldsymbol{d}^\star = \underset{\boldsymbol{d} \, \in \, \mathbb{R}^{n_d}}{\operatorname{argmax}} \ \mathbb{E}_{\boldsymbol{p}|\boldsymbol{d}} \left[D_{\mathrm{KL}}([\boldsymbol{q}|\boldsymbol{p}, \boldsymbol{d}] \parallel [\boldsymbol{q}]) \right] \ . \tag{14}$$

For normal linear regression models, which is the case here, the expected utility (14) is known as the Bayesian D-optimality criterion [11] and admits a closed form expression.

3. Sequential approach for the positioning of microphone arrays

This section introduces a sequential approach to acquire several measurements iteratively. This approach improves the reconstruction of the source field by finding at each step the best microphone array position.

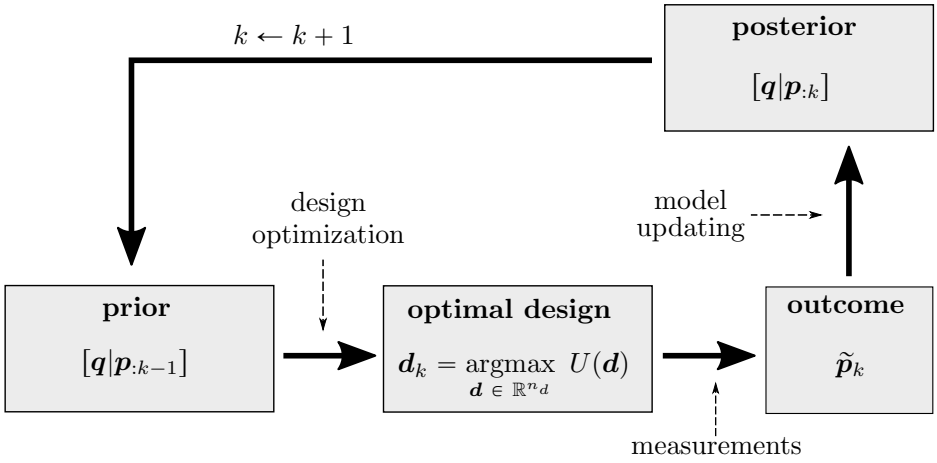

Figure 2: Scheme of the sequential approach for the positioning of microphone arrays.

3.1. Sequential formulation

Consider sets of measurements acquired over K consecutive experiments $(\widetilde{\boldsymbol{p}}_0, \ldots, \widetilde{\boldsymbol{p}}_K)$, where each set has been captured by an array of M_k microphones,

$$\widetilde{\boldsymbol{p}}_k = (\widetilde{p}_k(\boldsymbol{r}_0), \ldots, \widetilde{p}_k(\boldsymbol{r}_{M_k})) \ , \qquad k = 1, \ldots, K \ .$$

In this manner, the result of all previous experiments are used to plan the next one. Note that, for the sake of generality, the number of microphones used, M_k, may vary from one iteration to another. The whole set of measurements obtained at the end of the first k experiments is denoted by $\boldsymbol{p}_{:k} = (\boldsymbol{p}_0, \ldots, \boldsymbol{p}_k)$.

Figure 2 illustrates the steps involved in one iteration of the proposed approach. Starting from an initial experiment $\boldsymbol{d}_0$, the set of measurements $\widetilde{\boldsymbol{p}}_0$ is used to perform inference on the source model parameters $\boldsymbol{q}$. This is the step called "model updating" in Fig. 2.

The resulting posterior distribution $[\boldsymbol{q}|\boldsymbol{p}_0]$ is then inputted in the "design optimization" step to search for the optimal position of the next microphone array, noted $\boldsymbol{d}_1$. Once this position has been found, the experiment is conducted to obtain a new set of measurements $\widetilde{\boldsymbol{p}}_1$. The whole process is then repeated with all the measurements at hand $\widetilde{\boldsymbol{p}}_{:1} = (\widetilde{\boldsymbol{p}}_0, \widetilde{\boldsymbol{p}}_1)$. The two steps "model updating" and "design optimization" are detailed hereafter.

The step "model updating" simply consists in applying the Bayesian focusing procedure of Section 2.1 to update the state of the source model, or in others words to reconstruct the source field with all the measurements at

hand. At iteration k, the Bayesian model is updated based on the set of measurements $\widetilde{\boldsymbol{p}}_{:k} = (\widetilde{\boldsymbol{p}}_0, \widetilde{\boldsymbol{p}}_1, \ldots, \widetilde{\boldsymbol{p}}_{k-1}, \widetilde{\boldsymbol{p}}_k)$ and yields a new posterior distribution modeling the reconstructed source field, $[\boldsymbol{q}|\boldsymbol{p}_{:k}]$.

Following the model update, the "design optimization" is nothing else than the search for the next optimal experiment. It relies on the expected utility criterion of Section 2.2.2, modified to reflect the sequential nature of the present approach. As such, the next position is sought as,

$$\boldsymbol{d}_{k+1} = \underset{\boldsymbol{d} \in \mathbb{R}^{n_d}}{\operatorname{argmax}} \; \mathbb{E}_{\{\mathcal{C}_{k+1}\}} \left[D_{\mathrm{KL}} \left([\boldsymbol{q}|\boldsymbol{p}_{:k+1}, \boldsymbol{d}] \parallel [\boldsymbol{q}|\boldsymbol{p}_{:k}, \boldsymbol{d}] \right) \right] \ , \tag{15}$$

with the condition: $\mathcal{C}_{k+1} = \boldsymbol{p}_{k+1}|\boldsymbol{p}_{:k} = \widetilde{\boldsymbol{p}}_{:k}, \boldsymbol{d}$. Although Eq. (15) is a little more complex than Eq. (14), the interpretation remains the same: if the KL divergence is close to zero for a candidate position $\boldsymbol{d}$, then the measurements that will be acquired at this position will not contribute to a meaningful update of the source model.

3.2. Search criterion

One can derive a closed-form expression for the search criterion (15). This section only outlines the main results, while the full development is provided in Appendix A. First, recall the KL divergence expression:

$$D_{\mathrm{KL}} \left([\boldsymbol{q}|\boldsymbol{p}_{:k+1}, \boldsymbol{d}] \parallel [\boldsymbol{q}|\boldsymbol{p}_{:k}, \boldsymbol{d}] \right) = \int_{\Theta} [\boldsymbol{q}|\boldsymbol{p}_{:k+1}, \boldsymbol{d}] \ln \left(\frac{[\boldsymbol{q}|\boldsymbol{p}_{:k+1}, \boldsymbol{d}]}{[\boldsymbol{q}|\boldsymbol{p}_{:k}, \boldsymbol{d}]} \right) d\boldsymbol{q} \ . \tag{16}$$

Owing to Bayes rule, Eq. (16) is reformulated in terms of the evidence. Then, the associated expected utility reads:

$$\begin{aligned} \mathrm{U}(\boldsymbol{d}) &= \mathbb{E}_{\{\mathcal{C}_{k+1}\}} \left[D_{\mathrm{KL}} \left([\boldsymbol{q}|\boldsymbol{p}_{:k+1}, \boldsymbol{d}] \parallel [\boldsymbol{q}|\boldsymbol{p}_{:k}, \boldsymbol{d}] \right) \right] \ , \\ \mathrm{U}(\boldsymbol{d}) &= -\mathbb{E}_{\{\mathcal{C}_{k+1}\}} \left[\mathrm{H} \left(\boldsymbol{p}_{k+1}|\boldsymbol{q}, \boldsymbol{d} \right) \right] + \mathrm{H} \left(\boldsymbol{p}_{k+1}|\boldsymbol{p}_{:k} = \widetilde{\boldsymbol{p}}_{:k}, \boldsymbol{d} \right) \ , \end{aligned} \tag{17}$$

where H(.) denotes the entropy function of a random variable. Given the distributions studied, the entropy terms of Eq. (17) can be further simplified, which results in the following expression of the expected utility,

$$\mathrm{U}(\boldsymbol{d}) \propto \log \left(\det \Sigma_{k+1}(\boldsymbol{d}) \right) \ , \tag{18}$$

where $\Sigma_{k+1}(\boldsymbol{d})$ is the covariance matrix of $\boldsymbol{p}_{k+1}|\boldsymbol{p}_{:k} = \widetilde{\boldsymbol{p}}_{:k}, \boldsymbol{d}$ and $\propto$ is the proportionality symbol. Thus, finding the next position only amounts to evaluate the determinant of a covariance matrix over the space of candidate positions,

$$\boldsymbol{d}_{k+1}^{(1)} = \underset{\boldsymbol{d} \in \mathbb{R}^{n_d}}{\operatorname{argmax}} \; \log \left(\det \Sigma_{k+1}(\boldsymbol{d}) \right) \ . \tag{19}$$

Algorithm 1 Sequential approach for the positioning of microphone arrays

choose $\boldsymbol{d}_0$
get measurements $\widetilde{\boldsymbol{p}}_0$
"model updating" step : $[\boldsymbol{q}|\boldsymbol{p}_0, \boldsymbol{d}]$
set: $k \leftarrow 1$, $stop \leftarrow false$
while !$stop$ **do**
    "design optimization" step: $\boldsymbol{d}_k$
    get measurements : $\widetilde{\boldsymbol{p}}_k$
    "model updating" step: $[\boldsymbol{q}|\boldsymbol{p}_{:k}, \boldsymbol{d}]$
    $k \leftarrow k + 1$
end while

The detailed expression of $\Sigma_{k+1}(\boldsymbol{d})$ is provided in Appendix A. Equation (19) is a classical result of the BED literature. Only, in the present context, it is lacking as reading through the expression of $\Sigma_{k+1}(\boldsymbol{d})$ shows that the next optimal position does not explicitly depend on the measurements $\widetilde{\boldsymbol{p}}_{:k}$.

A possible alternative is to incorporate the cross spectral matrix of the reconstructed source field, $\widehat{\Sigma}_{\boldsymbol{q}}^{(k)}$. The details are also provided in Appendix A. In this case, the next position is expressed as,

$$\boldsymbol{d}_{k+1}^{(2)} = \underset{\boldsymbol{d} \in \mathbb{R}^{n_d}}{\operatorname{argmax}} \ \log\left(\det \widehat{\Sigma}_{k+1}(\boldsymbol{d})\right) \ , \tag{20}$$

where $\widehat{\Sigma}_{k+1}$ is a function of $\boldsymbol{d}$ and also depends on the cross spectral matrix $\widehat{\Sigma}_{\boldsymbol{q}}^{(k)}$. In the present paper, the search criterion considered is a weighted combination of the latter two criteria (19), (20),

$$\boldsymbol{d}_{k+1}^{\star} = \underset{\boldsymbol{d} \in \mathbb{R}^{n_d}}{\operatorname{argmax}} \ w \log\left(\det \Sigma_{k+1}(\boldsymbol{d})\right) + (1-w) \log\left(\det \widehat{\Sigma}_{k+1}(\boldsymbol{d})\right) \ . \tag{21}$$

The proposed criterion offers a balance between a first term that serves as a space-filling search criterion and a second one that seeks the space regions where the source directivity is maximal. This interpretation will be illustrated in Section 4. The weight w can be used to give more importance to either one of the two terms. In the following, $w = 1/2$ such that each term is equally important.

3.3. Algorithm

Algorithm 1 summarizes the main steps of the proposed sequential procedure. The two main points that have yet to be discussed are: the starting position $\boldsymbol{d}_0$ and the stopping criterion, *stop* in Algorithm 1.

The starting position can be selected by expertise or, if necessary, randomly. Better yet, if a former batch of measurements is available and the corresponding position of the array is known, one can directly jump to Step 3 of Algorithm 1. The impact of choosing the starting position at random should not be underestimated as it will be illustrated in Section 4.

The stopping criterion will probably be dictated given the nature of the application. In industrial applications, it is safe to assume that the number of iterations is budgeted. As such, the stopping criterion equals a maximum number of iterations. If there is no budget constraints, one could look at the KL divergence between the estimated source field at the current iteration k and at the previous iteration $k-1$. In the case of two complex normal distributions $\mathcal{CN}(\mu_0, \Sigma_0)$ and $\mathcal{CN}(\mu_1, \Sigma_1)$, the KL divergence reads:

$$D_{\mathrm{KL}} = -N + \mathrm{tr}\left(\Sigma_1^{-1}\Sigma_0\right) + \ln\left(\frac{\det\Sigma_1}{\det\Sigma_0}\right) + (\mu_1-\mu_0)^{\mathsf{H}}\Sigma_1^{-1}(\mu_1-\mu_0) \ , \quad (22)$$

where N is the dimension of each distribution. By plugging $\mathcal{CN}\left(\widehat{\mu}_{\boldsymbol{q}}^{(k)}, \widehat{\Sigma}_{\boldsymbol{q}}^{(k)}\right)$ and $\mathcal{CN}\left(\widehat{\mu}_{\boldsymbol{q}}^{(k-1)}, \widehat{\Sigma}_{\boldsymbol{q}}^{(k-1)}\right)$ in place of $\mathcal{CN}(\mu_0, \Sigma_0)$ and $\mathcal{CN}(\mu_1, \Sigma_1)$, one can check if the KL divergence is lower than a specified threshold and decide whether to stop the algorithm or carry on.

3.4. Multi-frequency case

So far, the proposed sequential approched has been formulated for a fixed frequency, f. In a real setting however, the experiment cannot be conducted one frequency at a time. The sequential formulation introduced in Section 3.1 as well as its search criterion need to be adapted to deal with multiple frequencies at once. The new aim becomes to find optimal positions of microphone arrays for a set of frequencies.

Figure 3 illustrates the mechanism of the multi-frequency case. The principle is to conduct the original sequential approach for each frequency in the set. Then, by making use of the KL divergence additive property, a single search criterion is built that combines the information extracted from each frequency in the set.

As a result, the search criterion of the sequential approach for the multi-frequency case reads:

$$\mathrm{U}(\boldsymbol{d}) = \sum_{\ell=1}^{F} \mathrm{U}_{f_\ell}(\boldsymbol{d}) \ , \quad (23)$$

where $\mathrm{U}_{f_\ell}(\boldsymbol{d})$ denotes the expected utility for the ℓ-th frequency in the set.

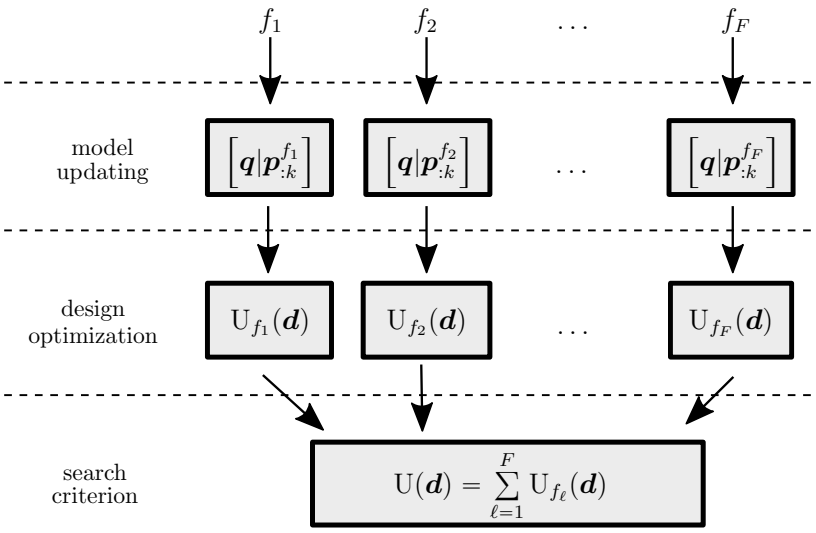

Figure 3: Scheme of the adapted sequential approach at the k-th iteration for the frequency set $\{f_0, f_1, \ldots, f_F\}$.

4. Application: directive source

4.1. Context and apparatus

This section illustrates the sequential approach of Section 3 for a highly directive source. One seeks to reconstruct the source directivity with 9 microphone array measurements. The successive positioning for the array are chosen among 900 positions around the source. The results are compared with a situation where the 9 successive positionings are set manually or randomly.

4.1.1. Directive source synthesis

A directive source is synthesized with a fifty point-sources spherical array. The nodes follow a Lebedev quadrature [20]. The spherical array is of radius $r_s = 0.05$ m. To compute the point-sources debits $\boldsymbol{q}$, a spherical harmonics expansion is used. Details are provided in Appendix B. The source main lobe has a steering angle of $(\theta_0 = 45°, \phi_0 = 0°)$ (the ϕ angle is taken from the equatorial plane). Its directivity pattern is shown in Fig. 5. (a) in solid line.

4.1.2. Microphone array configuration

To map sequentially the sound pressure field radiated by the directive source, a circular microphone array with 36 microphones is used. It consists

of 3 concentric rings of microphones, equally spaced along the azimuth angle, as shown in Fig. 4(a).

4.1.3. Signal to noise ratio

The microphone pressure signals $\boldsymbol{p}$ are simulated using Eq. (1), where the computation of the source debits strengths $\boldsymbol{q}$ are detailed in Appendix B and the noise vector is simulated with,

$$n_i = 10^{-\mathrm{SNR}/20} \, |A_i| \, \mathrm{e}^{\jmath B_i} \sqrt{\frac{\|\boldsymbol{p}_0\|_2^2}{M}} \ , \qquad i = 1, \ldots, M \ , \tag{24}$$

where A_i and B_i are two independent random variables following respectively a standard normal distribution and a uniform distribution on $[0, 2\pi]$ and the signal-to-noise ratio (SNR) is set equal to 10.

4.1.4. Reconstruction surface

The debit strengths $\boldsymbol{q}$ are estimated on a spherical surface of radius $r_s = 0.05$ m, sampled with 400 nodes following a Fliege grid [21]. It is represented in Fig. 4-(b). Note that the reconstruction surface has the same radius as the spherical point-sources array, but does not contain the exact location of the point-sources.

4.1.5. Search space for iterative positioning

The search space for the microphone array positioning, represented in Fig. 4-(c), is a spherical surface sampled with 900 nodes following a Fliege grid [21]. In the reported case, one chooses to constraint the microphone array orientation such that the plane containing the microphones (defined with vector $\mathbf{u}$ and $\mathbf{v}$ in Fig. 1) is tangent to the 900-node spherical surface. Therefore, the microphone array positioning $\boldsymbol{d}$ is entirely defined by the spherical coordinates $(r_a = 0.5 \text{ m}, \theta, \phi)$.

Finally, at each iteration, 900 candidate positions $\boldsymbol{d}$ are considered, and the one maximizing the expected utility $\mathrm{U}(\boldsymbol{d})$ of Eq. (19) is retained. The initial positioning, $\boldsymbol{d}_0$ is chosen randomly among the 900 possible position. In the reported case, its values are $\boldsymbol{d}_0 = (r = 0.5 \text{ m}, \theta = 0.732 \text{ rad}, \phi = 0.339 \text{ rad})$.

4.1.6. Reconstruction quality evaluation

To gauge the quality of the reconstruction, the estimated source field is propagated towards the aforementioned search space. Then, a normalized

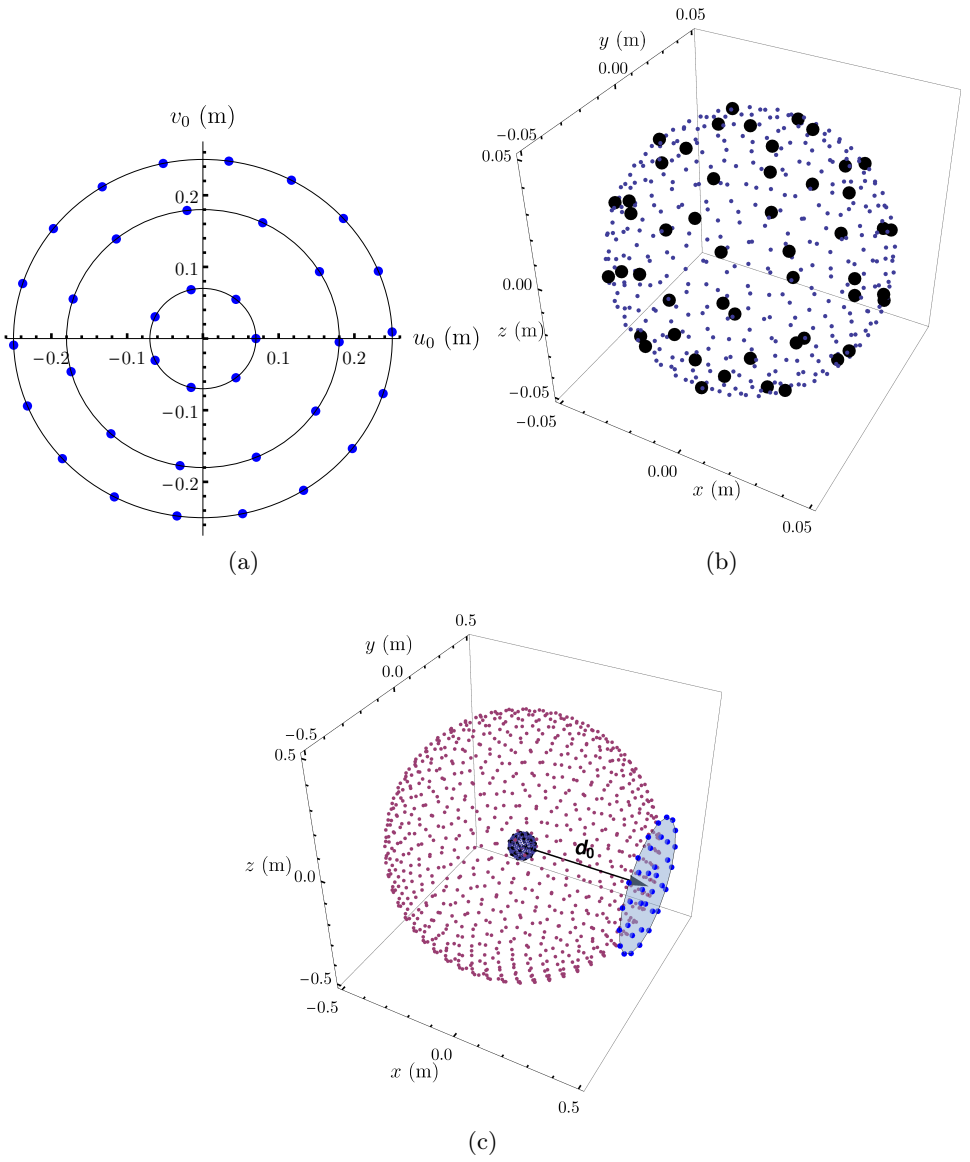

Figure 4: Scheme of the numerical setting: (a) Microphone array represented in the coordinate system ($\boldsymbol{d}_0$, u_0, v_0, w_0) of Fig. 1. (b) spherical surface of the studied source discretized into 400 points (small dots) and positions of the 50 loudspeakers (big dots). (c) Array of 900 points modeling the search space, source and reconstruction points in the middle, and microphone array placed at initial position $\boldsymbol{d}_0$.

mean square error between the theoretical pressures and the reconstructed ones is evaluated (in percent):

$$\text{MSE}(\%) = 100 \times \frac{\|\boldsymbol{p}_t - \widehat{\boldsymbol{p}}\|_2}{\|\boldsymbol{p}_t\|_2} \ , \tag{25}$$

where $\|.\|_2$ denotes the Euclidean norm, $\boldsymbol{p}_t$ and $\widehat{\boldsymbol{p}}$ denote respectively the theoretical and reconstructed pressures on the 900-nodes array.

4.2. Results for a single frequency

Figure 5 gathers the results of the sequential approach at frequency $f = 2000$ Hz after the 9 iterations. Figure 5-(a) shows a polar plot in the horizontal plane ($\phi = 0$) of both the theoretical (straight line) and the estimated (dashed line) normalized acoustic pressure directivities (in dB) at $0.5\,m$. It can be observed that the reconstructed directivity captures well the main lobe with some discrepancies in the side lobes that can be considered negligible given the respective dB levels.

Figure 5-(b) shows the evolution of the MSE, on a logarithmic scale, along the iterations. The MSE almost continuously decreases at an exponential rate. At the 9th iteration, the MSE is lower than 8% (≈ -10 dB).

Figures 5-(c,d) show respectively the theoretical and reconstructed acoustic sound pressure level (dB ref 1), in the horizontal plane ($\phi = 0$). The reconstructed pressure captures well the true directivity of the source in the direction $\theta = \pi/4$.

4.2.1. Interpretation of the search criterion

In Section 3.2, it has been said that the search criterion is composed of two terms: a first one allowing the exploration of the space of candidate positions for the microphone array, and a second one focusing on the main lobes of the source directivity. This interpretation is illustrated in Fig. 6 that displays the positions obtained by each of the 9 iterations, for each of the three criteria: $\boldsymbol{d}_{k+1}^{(1)}$ (Eq. (19)), $\boldsymbol{d}_{k+1}^{(2)}$ (Eq. (20)) and $\boldsymbol{d}_{k+1}^{\star}$ (Eq. (21)). The contour lines represent the directivity of the source on the search space, that is the array of 900 microphones displayed in Fig 3-(b).

One can observe that the positions $\boldsymbol{d}_{k+1}^{(2)}$ are clustered in and around the region where the main lobes are found. On the other hand, the positions $\boldsymbol{d}_{k+1}^{(1)}$ are evenly spread in the search space. The positions $\boldsymbol{d}_{k+1}^{\star}$ are balanced, some being located near the directivity peak, others allowing the exploration of the rest of the search space.

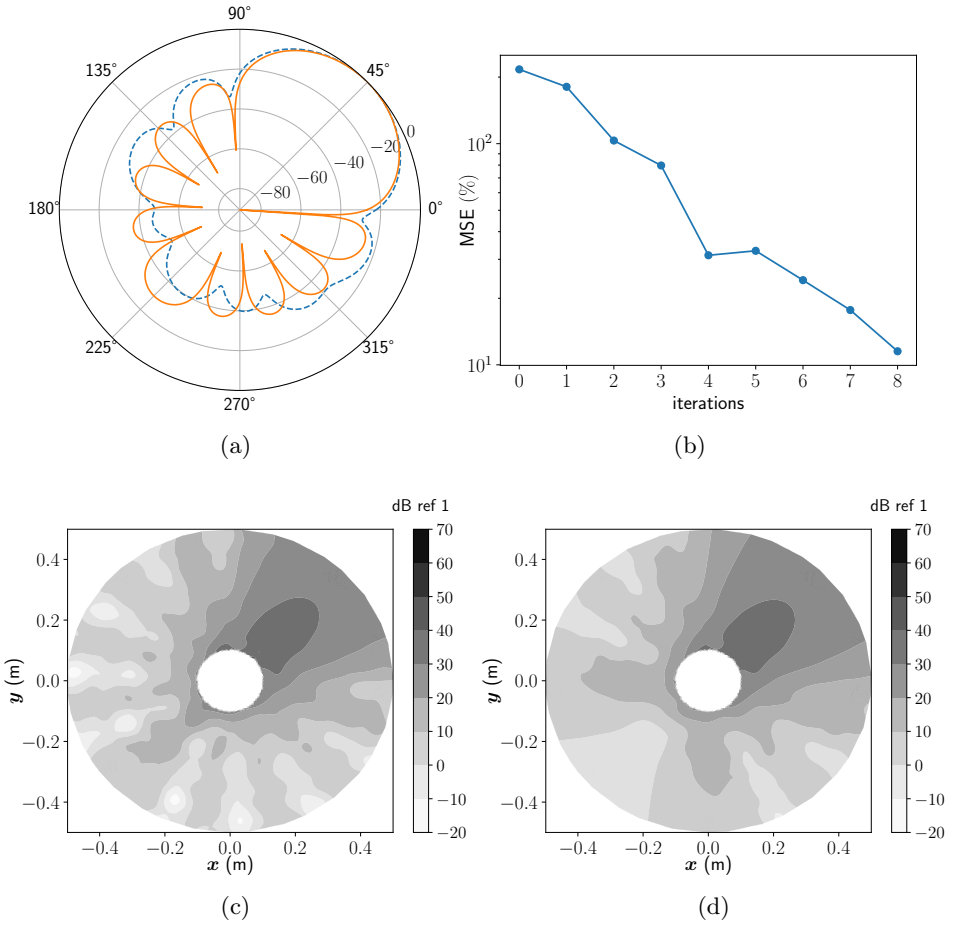

Figure 5: Simulation results at $f = 2000$ Hz: (a) polar plot in the horizontal plane ($\phi = 0$) of both the normalized theoretical acoustic pressure directivity (straight line) and the normalized reconstructed acoustic pressure directivity (dashed line) at $r_a = 0.5$ m. (b) Evolution of the MSE (in logarithmic scale) over the 10 iterations. (c) theoretical and (d) reconstructed acoustic pressure level, in dB ref 1, in the horizontal plane ($\phi = 0$).

4.2.2. Impact of the starting position

The starting position $\boldsymbol{d}_0$ can have a non-negligible impact on the speed of the algorithm if chosen at random. To illustrate this point, 100 runs of 9 iterations are performed while randomly selecting the starting position of each run. Then, the MSE of Eq. (25) is evaluated for each run.

Figure 7 presents the curves, in logarithmic scale, of the MSE obtained for the 100 runs as well as the original curve (dashed line) displayed in Fig. 4-(b). One can observe significant discrepancies between the curves in the

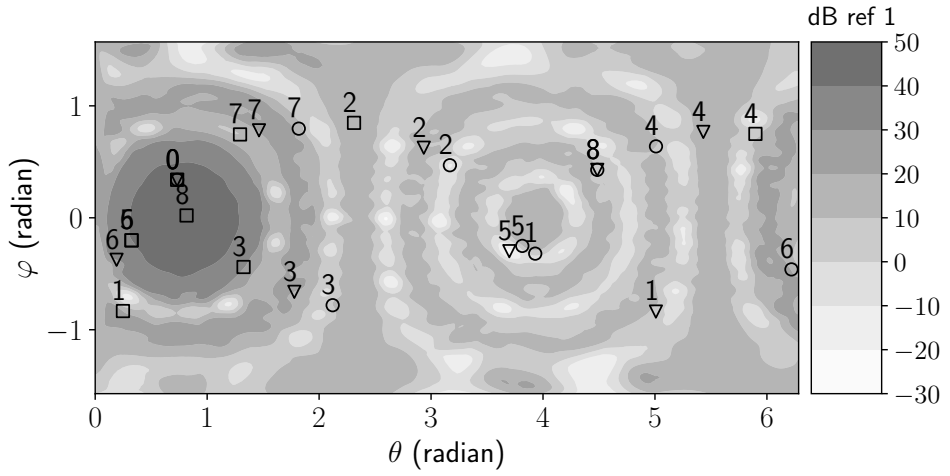

Figure 6: Plot of the positions obtained by each of the 9 iterations for the following three criteria: $\boldsymbol{d}_{k+1}^{(1)}$ (black dots), $\boldsymbol{d}_{k+1}^{(2)}$ (black squares) and $\boldsymbol{d}_{k+1}^{\star}$ (black triangles). The contour lines represent the sound pressure level in dB ref 1.

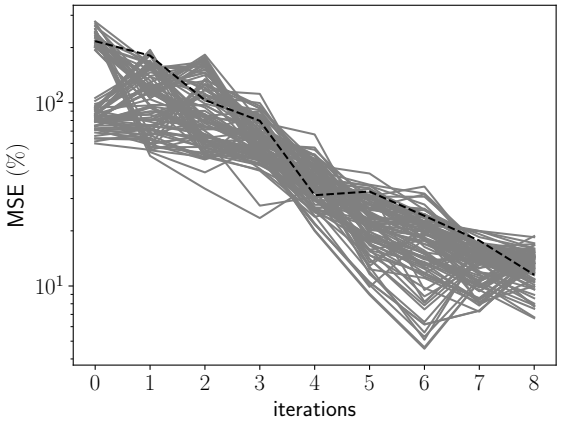

Figure 7: Curves (in logarithmic scale) of the MSE for 100 runs of 9 iterations where the starting position is selected at random. The gray curves correspond to the MSE evaluated for the runs and the dashed curve represents the MSE of the sequential approach.

first iterations, which rapidly shrink after the 6th-7th iterations. As such, one should pay attention to the starting position if the number of iterations is a concern.

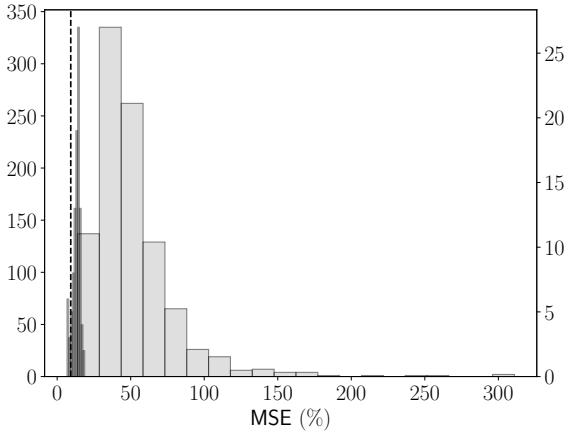

Figure 8: Histogram of the MSE sample obtained from 1000 runs of the "blindfolded" approach. The black histogram represents the 100 MSE final values (with random initialization) of Fig. 7. The black vertical dashed line represents the MSE value (12.43 %) obtained with the deterministic approach.

4.2.3. Comparison with a blindfolded approach

To conclude this section, a comparison between the proposed sequential procedure and a "blindfolded" approach is performed. Here, the term "blindfolded" refers to an approach ignoring the procedure introduced in Section 3, where instead the 9 positions of the microphone array are selected all-together, the measurements are acquired in one shot and the Bayesian focusing procedure (see Section 2.1) is applied a single time to estimate the source field.

The most classical "blindfolded" approach consists in randomly selecting the 9 positions of the microphone array. 1000 runs of this random approach are performed and the MSE (Eq. (25)) is used to assess the quality of the source field reconstruction for each run. Additionally, a deterministic approach is considered, where the 9 positions are given by a Fliege spherical array [21].

Figure 8 presents a histogram of the MSE sample obtained from the 1000 runs. Additionally, the 100 MSE final values (with random initialization) of Fig. 7, are represented by a black histogram. The MSE value obtained with the deterministic approach is highlighted by a black vertical dashed line. It is clearly shown that the proposed sequential approach performs better than a classical one based on a random selection of the positions of the microphone array and close to the deterministic approach. Note that the latter happens to perform particularly well in this case since one of the nine positions is

	Steering angle coordinates	
frequency (Hz)	θ (radian)	ϕ (radian)
500	$\pi/2$	$\pi/4$
1000	$7\pi/20$	$3\pi/20$
1500	$\pi/5$	$\pi/20$
2000	$\pi/20$	$-\pi/20$
2500	$-7\pi/10$	$-3\pi/20$
3000	$-\pi/4$	$-\pi/4$

Table 1: Coordinates of the steering angle of the source main lobe for each frequency in the set $\mathcal{B}_f = \{500, 1000, 1500, 2000, 2500, 3000\}$.

located at the center of the source main lobe.

4.3. Results for a frequency set

This section illustrates the sequential approach with multiple frequencies at once, for the same source model introduced in Section 4.1. The aim is still to reconstruct accurately the directivity of the source at $r = 0.5$ m. The frequency set considered is $\mathcal{B}_f = \{500, 1000, 1500, 2000, 2500, 3000\}$. The directivity of the source varies with the frequency. Table 1 lists the coordinates of the steering angle of the source main lobe per frequency studied.

The numerical setting is the same as the one described in Section 4.2 and illustrated in Fig. 3. Once again, the normalized MSE of Eq. (25) is used to assess the quality of the source estimation. The only difference is that one MSE curve is obtained per frequency, $\text{MSE}_f, f \in \mathcal{B}_f$.

A fixed number of 9 iterations is chosen and the microphone array used to acquire the measurement at each iteration is the same circular array of 36 microphones. The simulation parameters are the same as in 4.2 except the search criterion which is now the one introduced in Section 3.4.

The results of the sequential approach are displayed in Figs. 9 - 10. Figure 9 shows, on a logarithmic scale, the curves of the MSE for each frequency in the set $\mathcal{B}_f$ while Fig. 10 represents the theoretical and reconstructed 3D-directivities at 1000, 2000 and 3000 Hz. These two figures highlight a good performance of the proposed approach. At the ninth iteration, values of the MSE range from 5.6% to 11.0%. Figure 10 shows that the reconstructed directivity matches well the theoretical one in the 3D-region containing the source main lobe.

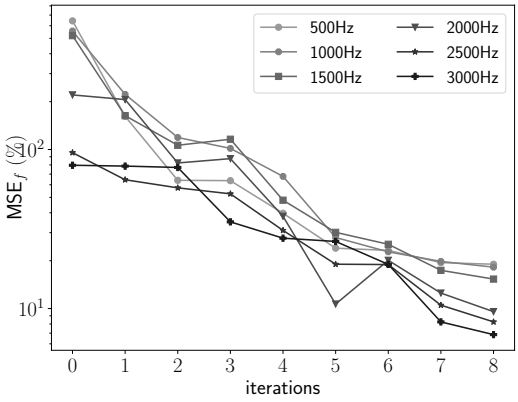

Figure 9: Curves (in logarithmic scale) of the MSE for each frequency in the set $\mathcal{B}_f$.

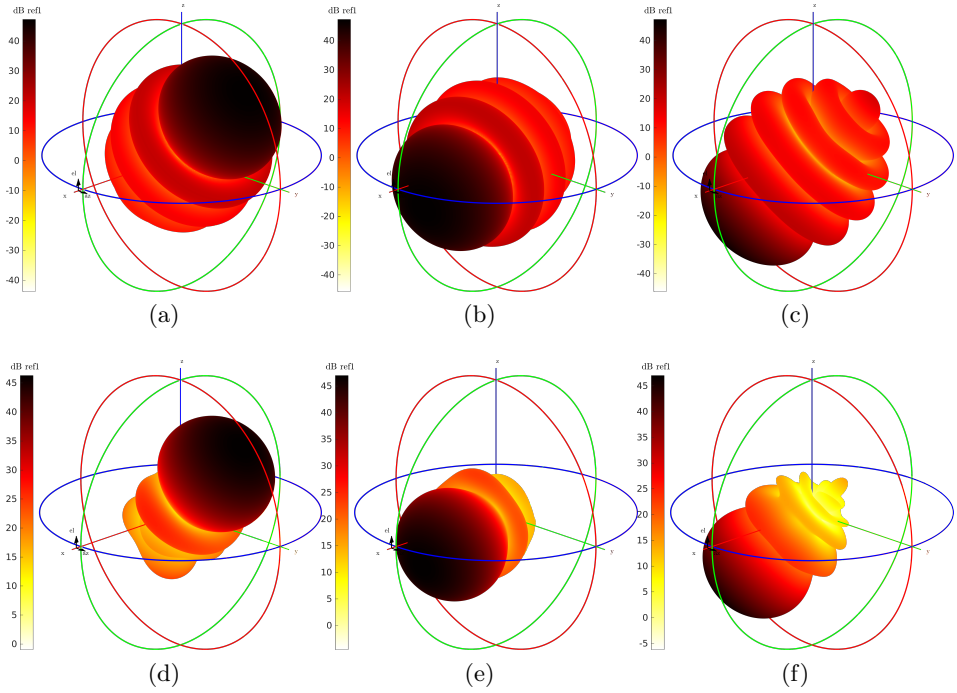

Figure 10: Theoretical sound pressure level, in dB ref 1, at $r_a = 0.5$ m and at frequencies a) 1000 Hz, b) 2000 Hz, c) 3000 Hz. Reconstructed sound pressure level, in dB ref 1, at $r_a = 0.5$ m and at frequencies d) 1000 Hz, e) 2000 Hz, f) 3000 Hz with the proposed sequential approach.

5. Conclusion

An efficient approach has been proposed in this paper to sequentially select optimal positions of microphone arrays. The Bayesian roots of the approach has made possible to formulate the search criterion as a closed-form expression derived from the Kullback-Leibler divergence between the prior and posterior distributions. Two versions of the approach have been presented, one for a single frequency case, and the other one encompasses configurations where measurements are acquired over a frequency band.

Through the study of a source synthesized with a fifty-nodes spherical array, the proposed approach has been shown to perform particularly well on both the single and multiple frequencies cases. An illustration of the search criterion mechanism has been given, displaying the balance it offers between an exploration of the search space, i.e. the space of the candidate positions, and a focus on the regions where lie the main lobes of the source directivity.

In addition, the proposed approach has been compared against "blind-folded" alternatives were positions of the microphone array are randomly selected and an ideal deterministic approach where the positions are given as the integration nodes of Fliege and Maier, with one node coinciding with the source main lobe. Results of the comparison highlighted the performance of the proposed approach, showing that it performs much better than random alternatives and, depending on the starting position, equally well as the deterministic approach.

Two remaining features have yet to be discussed. First, the design optimization step has been carried out by simply choosing the best candidate after discretization of the search space. Nevertheless, it is important to note that the approach itself is completely autonomous from the choice of the optimization algorithm. One could consider alternatives, for instance meta-model techniques to fit a response surface.

Secondly, the choice of the set for the multi-frequency case must be taken with care as the algorithm is expected to be limited by the spatial aliasing of the antenna. A situation prone to errors would be one where a frequency selected outside the microphone array bandwidth would drive the search criterion. One suggestion to circumvent this issue is to apply a set of frequency-dependent weights to the search criterion to lessen the impact of the frequency band limits.

Acknowledgments

This work was supported by the LUG2 project funded by the Région Auvergne Rhône-Alpes and the BPIFrance (grant FUI22). This work was per-

formed within the framework of the Labex CeLyA of Université de Lyon, operated by the French National Research Agency (ANR-10-LABX-0060/ANR-11-IDEX-0007).

Appendix A. Search criterion

This section develops the theoretical background to obtain the closed-form expression, given in Eq. (19), of the search criterion. Owing to Bayes rule,

$$[\boldsymbol{q}|\boldsymbol{p}_{:k+1},\boldsymbol{d}] = [\boldsymbol{q}|\boldsymbol{p}_{k+1},\boldsymbol{p}_{:k},\boldsymbol{d}] = \frac{[\boldsymbol{p}_{k+1}|\boldsymbol{q},\boldsymbol{d}]\,[\boldsymbol{q}|\boldsymbol{p}_{:k},\boldsymbol{d}]}{[\boldsymbol{p}_{k+1}|\boldsymbol{p}_{:k},\boldsymbol{d}]}\ . \tag{A.1}$$

The KL divergence of Eq. (16), hereafter abbreviated by D_{KL}, is reformulated as follows:

$$D_{\mathrm{KL}} = \int_{\Theta} \frac{[\boldsymbol{p}_{k+1}|\boldsymbol{q},\boldsymbol{d}]\,[\boldsymbol{q}|\boldsymbol{p}_{:k},\boldsymbol{d}]}{[\boldsymbol{p}_{k+1}|\boldsymbol{p}_{:k},\boldsymbol{d}]} \ln\left(\frac{[\boldsymbol{p}_{k+1}|\boldsymbol{q},\boldsymbol{d}]}{[\boldsymbol{p}_{k+1}|\boldsymbol{p}_{:k},\boldsymbol{d}]}\right) d\boldsymbol{q}\ . \tag{A.2}$$

Then, the associated expected utility reads:

$$\begin{aligned}
\mathrm{U}(\boldsymbol{d}) &= \mathbb{E}_{\{\boldsymbol{p}_{k+1}|\boldsymbol{p}_{:k}=\widetilde{\boldsymbol{p}}_{:k},\boldsymbol{d}\}}\left[D_{\mathrm{KL}}\right]\ , \\
\mathrm{U}(\boldsymbol{d}) &= \int_{\Theta} [\boldsymbol{q}|\boldsymbol{p}_{:k}=\widetilde{\boldsymbol{p}}_{:k},\boldsymbol{d}] \left(\int_{\mathcal{P}} [\boldsymbol{p}_{k+1}|\boldsymbol{q},\boldsymbol{d}] \ln\left([\boldsymbol{p}_{k+1}|\boldsymbol{q},\boldsymbol{d}]\right) d\boldsymbol{p}_{k+1}\right) d\boldsymbol{q} \\
&- \int_{\mathcal{P}} [\boldsymbol{p}_{k+1}|\boldsymbol{p}_{:k}=\widetilde{\boldsymbol{p}}_{:k},\boldsymbol{d}] \ln\left([\boldsymbol{p}_{k+1}|\boldsymbol{p}_{:k}=\widetilde{\boldsymbol{p}}_{:k},\boldsymbol{d}]\right) d\boldsymbol{p}_{k+1}\ , \\
\mathrm{U}(\boldsymbol{d}) &= -\int_{\Theta} [\boldsymbol{q}|\boldsymbol{p}_{:k}=\widetilde{\boldsymbol{p}}_{:k},\boldsymbol{d}]\,\mathrm{H}(\boldsymbol{p}_{k+1}|\boldsymbol{q},\boldsymbol{d})d\boldsymbol{q} + \mathrm{H}(\boldsymbol{p}_{k+1}|\boldsymbol{p}_{:k}=\widetilde{\boldsymbol{p}}_{:k},\boldsymbol{d})\ , \\
\mathrm{U}(\boldsymbol{d}) &= -\mathbb{E}_{\{\boldsymbol{q}|\boldsymbol{p}_{:k}=\widetilde{\boldsymbol{p}}_{:k},\boldsymbol{d}\}}\left[\mathrm{H}(\boldsymbol{p}_{k+1}|\boldsymbol{q},\boldsymbol{d})\right] + \mathrm{H}(\boldsymbol{p}_{k+1}|\boldsymbol{p}_{:k}=\widetilde{\boldsymbol{p}}_{:k},\boldsymbol{d})\ .
\end{aligned} \tag{A.3}$$

where H(.) denotes the entropy function of a random variable. It suffices to remark that the entropy term $\mathrm{H}(\boldsymbol{p}_{k+1}|\boldsymbol{q},\boldsymbol{d})$ is independent from $\boldsymbol{q}$ and $\boldsymbol{d}$, that is the first term is a constant c. Then, given that $\boldsymbol{p}_{k+1}|\boldsymbol{p}_{:k},\boldsymbol{d}$ follows a complex normal distribution,

$$[\boldsymbol{p}_{k+1}|\boldsymbol{p}_{:k}=\widetilde{\boldsymbol{p}}_{:k},\boldsymbol{d}] = \mathcal{CN}(\mu_k(\boldsymbol{d}),\Sigma_{k+1}(\boldsymbol{d}))\ , \tag{A.4}$$

the second term is proportional to:

$$\mathrm{H}(\boldsymbol{p}_{k+1}|\boldsymbol{p}_{:k},\boldsymbol{d}) \propto \log\left(\det\Sigma_{k+1}(\boldsymbol{d})\right)\ , \tag{A.5}$$

which is the result of Eq. (18).

The expression of $\Sigma_{k+1}(\boldsymbol{d})$ is obtained from the two equations,

$$\boldsymbol{p}_{:k} = \boldsymbol{G}_{:k}(\boldsymbol{d})\boldsymbol{q} + \boldsymbol{n}_{:k} \ , \qquad \boldsymbol{p}_{k+1} = \boldsymbol{G}_{k+1}(\boldsymbol{d})\boldsymbol{q} + \boldsymbol{n}_{k+1} \ . \tag{A.6}$$

The associated distributions are: $[\boldsymbol{q}] = \mathcal{CN}(\boldsymbol{0}, \Sigma_{\boldsymbol{q}}^{(k)})$, $[\boldsymbol{n}_{:k}] = \mathcal{CN}(\boldsymbol{0}, \beta^2 I_{\boldsymbol{n}_{:k}})$, $[\boldsymbol{n}_{k+1}] = \mathcal{CN}(\boldsymbol{0}, \beta^2 I_{\boldsymbol{n}_{k+1}})$, with

$$\Sigma_{\boldsymbol{q}}^{(k)} = \left(\alpha^{-2} \left(\Sigma_{\boldsymbol{q}}^{(k-1)} \right)^{-1} + \beta^{-2} \boldsymbol{G}_{:k-1}^{\mathsf{H}} \boldsymbol{G}_{:k-1} \right)^{-1} . \tag{A.7}$$

It follows from this that,

$$\Sigma_{k+1}(\boldsymbol{d})) = \Sigma_{1,1} - \Sigma_{1,2} \Sigma_{2,2}^{-1} \Sigma_{1,2}^{\mathsf{H}} \ , \tag{A.8}$$

where:

$$\begin{cases} \Sigma_{1,1} = \alpha^2 \boldsymbol{G}_{k+1}(\boldsymbol{d}) \Sigma_{\boldsymbol{q}}^{(k)} \boldsymbol{G}_{k+1}^{\mathsf{H}}(\boldsymbol{d}) + \beta^2 I_{\boldsymbol{n}_{k+1}} \ , \\ \Sigma_{1,2} = \alpha^2 \boldsymbol{G}_{k+1}(\boldsymbol{d}) \Sigma_{\boldsymbol{q}}^{(k)} \boldsymbol{G}_{:k}^{\mathsf{H}}(\boldsymbol{d}) \ , \\ \Sigma_{2,2} = \alpha^2 \boldsymbol{G}_{:k}(\boldsymbol{d}) \Sigma_{\boldsymbol{q}}^{(k)} \boldsymbol{G}_{:k}^{\mathsf{H}}(\boldsymbol{d}) + \beta^2 I_{\boldsymbol{n}_{:k}} \ . \end{cases} \tag{A.9}$$

Then, the expression of $\widehat{\Sigma}_{k+1}(\boldsymbol{d})$ in Eq. (20) is simply obtained by substituting the cross spectral matrix of the reconstructed source field, $\widehat{\Sigma}_{\boldsymbol{q}}^{(k)}$, for $\Sigma_{\boldsymbol{q}}^{(k)}$ in Eq. (A.8).

Appendix B. Directive source with spherical harmonics

For the exterior problem where the acoustic sources are inside a sphere of radius r_s, the Helmholtz equation has its solution in spherical coordinate system given by [22]:

$$p(r, \theta, \phi) = \sum_{l=0}^{\infty} h_l^{(2)}(kr) \sum_{m=-l}^{l} C_{lm} Y_{lm}(\theta, \phi). \tag{B.1}$$

In Eq. (B.1), Y_{lm} are the 4-π normalized real spherical harmonics of degree l and order m, $h_l^{(2)}$ are the spherical Hankel functions of second kind, $k = 2\pi f/c$ is the wave number with f the frequency and c the sound speed. The spherical harmonics coefficients of the sound pressure field are denoted C_{lm}. As well, the free-field Green function is expressed as [22]:

$$\frac{\mathrm{e}^{-\mathrm{i}k|\mathbf{r}-\mathbf{r}_s|}}{4\pi|\mathbf{r}-\mathbf{r}_s|} = \frac{-\mathrm{i}k}{4\pi} \sum_{l=0}^{\infty} h_l^{(2)}(kr) j_l(kr_s) \sum_{n=-l}^{l} Y_{lm}(\theta_s, \phi_s) Y_{mn}(\theta, \phi), \tag{B.2}$$

where $\mathbf{r} = (r, \theta, \phi)$, is the measurement point location, $\mathbf{r}_s = (r_s, \theta_s, \phi_s)$ is the source point location, $\mathbf{r} > r_s$, and j_l are the spherical Bessel functions.

Appendix B.1. Continuous point-sources spherical distribution

Let's consider a continuous distribution of point-sources on an open sphere of radius r_s, centered at origin. The radiated pressure at $\mathbf{r}$ is given by:

$$\hat{p}(k, r, \theta, \phi) = \frac{1}{4\pi} \int_{\theta_s=0}^{2\pi} \int_{\phi_s=-\frac{\pi}{2}}^{\frac{\pi}{2}} q(r_s, \theta_s, \phi_s) \frac{\mathrm{e}^{-\mathrm{i}k|\mathbf{r}-\mathbf{r}_s|}}{4\pi|\mathbf{r}-\mathbf{r}_s|} \cos(\phi_s) d\phi_s d\theta_s, \quad \text{(B.3)}$$

where $\hat{p}(k, r, \theta, \phi)$ is the radiated pressure, $q(\theta_s, \phi_s)$ is the strength density at point $\mathbf{r}_s = (r_s, \theta_s, \phi_s)$. By inserting Eq. (B.2) in Eq. (B.3) and using the spherical harmonics orthonormality property, one can demonstrate that [22]:

$$q(r_s, \theta_s, \phi_s) = \sum_{l=0}^{\infty} \sum_{m=-l}^{l} \frac{4\pi C_{lm} Y_{lm}(\theta_s, \phi_s)}{-\mathrm{i}k j_l(kr_s)} \quad \text{(B.4)}$$

Note that in this case, some frequencies are forbidden corresponding to the zeros values of function $j_l(kr_s)$.

Appendix B.2. Directional Dirac

A directional Dirac delta is expressed as:

$$\delta(\theta - \theta_0, \phi - \phi_0) = \sum_{l=0}^{\infty} \sum_{m=-l}^{l} Y_{lm}(\theta, \phi) Y_{lm}(\theta_0, \phi_0) \quad \text{(B.5)}$$

This function is zero everywhere except at the steering angle (θ_0, ϕ_0). One seeks to reproduce this directivity at radius r_a. The radial propagation has to be compensated in Eq. (B.1), for the pressure at radius r_a to be equal at Eq. (B.5). Therefore, one chooses the coefficients C_{lm} in Eq. (B.1) such that:

$$C_{lm} = \frac{Y_{lm}(\theta_0, \phi_0)}{h_l^{(2)}(kr_a)} \quad \text{(B.6)}$$

Recalling Eq. (B.4) one has:

$$q(r_s, \theta_s, \phi_s) = \sum_{l=0}^{\infty} \sum_{m=-l}^{l} \frac{4\pi Y_{lm}(\theta_0, \phi_0) Y_{lm}(\theta_s, \phi_s)}{-\mathrm{i}k j_m(kr_s) h_m^{(2)}(kr_a)} \quad \text{(B.7)}$$

This equation is further simplified using the addition theorem for spherical harmonics [23]:

$$q(r_s, \theta_s, \phi_s) = \sum_{l=0}^{\infty} \frac{4\pi(2l+1)P_l(\cos(\Theta))}{-\mathrm{i}kj_l(kr_q)h_m^{(2)}(kr_a)}, \tag{B.8}$$

where P_l is the Legendre polynomial of degree l and Θ is the angle between a point source on the spherical surface and the steering angle (θ_0, ϕ_0). One has:

$$\cos(\Theta) = \frac{\mathbf{r}_s}{r_s} \cdot \frac{\mathbf{r}_0}{r_a}, \tag{B.9}$$

with $\mathbf{r}_0 = (r_a, \theta_0, \phi_0)$.

Appendix B.3. Max-r_E weighting

The directional Dirac source of Eq. (B.6) presents side lobes when the spherical harmonic decomposition is truncated up to maximum degree L. By weighting each component of the decomposition in Eq. (B.6), the side lobes can be attenuated sufficiently at the cost of a main-lobe widening with max-r_E weights [24]. To derive them for a maximum degree L, the first step is to find the highest root of Legendre polynomial P_{L+1}, denoted r_E:

$$P_{L+1}(r_E) = 0. \tag{B.10}$$

Then, the weights for each degree l are given by:

$$\alpha_l = P_l(r_E) \qquad l = 0, \ \cdots \ , L. \tag{B.11}$$

Finally, the source strengths of Eq. (B.8) are changed to:

$$q(r_s, \theta_s, \phi_s) = \sum_{l=0}^{\infty} \frac{\alpha_l 4\pi(2l+1)P_l(\cos(\Theta))}{-\mathrm{i}kj_l(kr_s)h_l^{(2)}(kr_a)}. \tag{B.12}$$

Appendix B.4. Discretization with a Lebedev grid

Lebedev provides nodes location and weights for the integration of spherical harmonics decompositions at various degree [20]. For instance, with $L = 50$ nodes, one can integrate exactly a product of spherical harmonics up to degree $L = 5$ [25]. Following this approach, the point sources distribution is now discrete. The q-th point-source coordinate is given by (r_s, θ_q, ϕ_q). Recalling Eq. (B.12), its strength is given by:

$$q(r_s, \theta_q, \phi_q) = \sum_{l=0}^{5} \frac{w_q \alpha_l 4\pi(2l+1)P_l(\cos(\Theta))}{-\mathrm{i}kj_l(kr_q)h_l^{(2)}(kr_a)} \qquad q = 1, \ \cdots \ , 50, \tag{B.13}$$

where w_q is the q-th node weight, given in [20, 25].

References

[1] D. C. Kammer, Sensor Placement for On-Orbit Modal Identification and Correlation of Large Space Structures, J. Guid. Control Dyn. 14 (1991) 251–259, doi:10.2514/3.20635.

[2] F. E. Udwadia, Methodology for Optimum Sensor Locations for Parameter Identification in Dynamic Systems, J. Eng. Mech. ASCE 120, doi:10.1061/(ASCE)0733-9399(1994)120:2(368).

[3] E. Heredia-Zavoni, R. Montes-Iturrizaga, L. Esteva, Optimal instrumentation of structures on flexible base for system identification, Earthq. Eng. Struct. D. 28 (12) (????) 1471–1482, doi:10.1002/(SICI)1096-9845(199912)28:12<1471::AID-EQE872>3.0.CO;2-M.

[4] C. Papadimitriou, Optimal sensor placement methodology for parametric identification of structural systems, J. Sound Vib. 278 (4) (2004) 923 – 947, doi:10.1016/j.jsv.2003.10.063.

[5] J. Zhang, K. Maes, G. D. Roeck, E. Reynders, G. Lombaert, Experimental verification of optimal sensor placement for multi-setup modal testing, Procedia Eng. 199 (2017) 1068 – 1073, doi:10.1016/j.proeng.2017.09.063.

[6] C. Stephan, Sensor placement for modal identification, Mech. Syst. Signal Process. 27 (2012) 461 – 470, doi:10.1016/j.ymssp.2011.07.022.

[7] Z. Li, R. Duraiswami, Flexible and Optimal Design of Spherical Microphone Arrays for Beamforming, IEEE Trans. Audio, Speech, Language Process. 15 (2) (2007) 702–714, doi:10.1109/TASL.2006.876764.

[8] G. Chardon, W. Kreuzer, M. Noisternig, Design of Spatial Microphone Arrays for Sound Field Interpolation, IEEE J. Sel. Topics Signal Process. 9 (5) (2015) 780–790, doi:10.1109/JSTSP.2015.2412097.

[9] J. Antoni, A Bayesian approach to sound source reconstruction: Optimal basis, regularization, and focusing, J. Acoust. Soc. Am. 131 (4) (2012) 2873–2890, doi:10.1121/1.3685484.

[10] S. Kullback, R. A. Leibler, On Information and Sufficiency, Ann. Math. Statist. 22 (1) (1951) 79–86, doi:10.1214/aoms/117772969.

[11] K. Chaloner, I. Verdinelli, Statist. Sci. 10 (3) (1995) 273–304, doi:10.1214/ss/1177009939.

[12] X. Huan, Y. M. Marzouk, Simulation-based optimal Bayesian experimental design for nonlinear systems, J. Comput. Phys. 232 (1) (2013) 288 – 317, doi:10.1016/j.jcp.2012.08.013.

[13] C. M. Ryan, C. C. Drovandi, A. N. Pettitt, Bayesian Anal. 11 (3) (2016) 857–883, doi:10.1214/15-BA977.

[14] W. Kim, M. A. Pitt, Z.-L. Lu, M. Steyvers, J. I. Myung, A Hierarchical Adaptive Approach to Optimal Experimental Design, Neural Comput. 26 (11) (2014) 2465–2492, doi:10.1162/NECO_a_00654.

[15] R. A. Wooding, The multivariate distribution of complex normal variables, Biometrika 43 (1-2) (1956) 212–215, doi:10.2307/2333597.

[16] P. C. Hansen, Rank-deficient and Discrete Ill-posed Problems: Numerical Aspects of Linear Inversion, Society for Industrial and Applied Mathematics, Philadelphia, PA, USA, 1998.

[17] A. Pereira, J. Antoni, Q. Leclère, Empirical Bayesian regularization of the inverse acoustic problem, Applied Acoustics 97 (Supplement C) (2015) 11–29, doi:10.1016/j.apacoust.2015.03.008.

[18] D. V. Lindley, Bayesian Statistics, A Review, Society for Industrial and Applied Mathematics, doi:10.1137/1.9781611970654, 1972.

[19] D. V. Lindley, Ann. Math. Statist. 27 (4) (1956) 986–1005, doi:10.1214/aoms/1177728069.

[20] V. I. Lebedev, Values of the Nodes and Weights of Quadrature Formulas of Gauss-Markov Type for a Sphere from the Ninth to Seventeenth Order of Accuracy That Are Invariant with Respect to an Octahedron, USSR Computational Mathematics and Mathematical Physics 15 (1) (1975) 44–51, doi:http://dx.doi.org/10.1016/0041-5553(75)90133-0.

[21] J. Fliege, U. Maier, The distribution of points on the sphere and corresponding cubature formulae, IMA Journal of Numerical Analysis 19 (2) (1999) 317–334, doi:10.1093/imanum/19.2.317.

[22] E. G. Williams, Fourier Acoustics: Sound Radiation And Nearfield Acoustical Holography, Academic Press, London, ISBN 0-12-753960-3, 1999.

[23] G. Arfken, Mathematical Methods for Physicists, Academic press, New York, 3rd edn., 1985.

[24] J. Daniel, J.-B. Rault, J.-D. Polack, Ambisonics Encoding of Other Audio Formats for Multiple Listening Conditions, in: Audio Engineering Society Convention 105, AES, San Francisco, 1–29, 1998.

[25] P. Lecomte, P.-a. Gauthier, C. Langrenne, A. Berry, A. Garcia, A Fifty-Node Lededev Grid and Its Applications to Ambisonics, Journal of the Audio Engineering Society 64 (11) (2016) 868–881.